ELSEVIER

n° 1-4

Chemical Geology 170 (2000) 19–35

CHEMICAL GEOLOGY
INCLUDING
ISOTOPE GEOSCIENCE

www.elsevier.com/locate/chemgeo

Chemical mass balance of calcrete genesis on the Toledo granite (Spain)

Arnaud Chiquet[a,*], Fabrice Colin[b], Bruno Hamelin[a], Annie Michard[a], Daniel Nahon[a]

[a] *CEREGE, UMR 6536, CNRS / Université Aix-Marseille III, BP 80, 13545 Aix-en-Provence, Cedex 04, France*
[b] *CEREGE, UMR 6536, ORSTOM / Université Aix-Marseille III, BP 80, 13545 Aix-en-Provence, Cedex 04, France*

Received 15 April 1998; accepted 12 May 1999

Abstract

The chemical mass balance of calcrete genesis is studied on a typical sequence developed in granite, in the Toledo mountains, Central Spain.

Field evidence and petrographic observations indicate that the texture and the bulk volume of the parent rock are strictly preserved all along the studied calcrete profile.

Microscopic observations indicate that the calcitization process starts within the saprolite, superimposed on the usual mechanisms of granite weathering: the fresh rock is first weathered to secondary clays, mainly smectites, which are then pseudomorphically replaced by calcite. Based on this evidence, chemical mass transfers are calculated, assuming iso-volume transformation from the parent rock to the calcrete.

The mass balance results show the increasing loss of matter due to weathering of the primary phases, from the saprolite towards the calcrete layers higher in the sequence. Zr, Ti or Th, which are classically considered as immobile during weathering, are also depleted along the profile, especially in the calcrete layer. This results from the prevailing highly alkaline conditions, which could account for the simultaneous precipitation of $CaCO_3$ and silicate dissolution.

The calculated budget suggests that the elements exported from the weathering profile are provided dominantly by the weathering of plagioclase and biotite. We calculate that 8–42% of the original Ca remains in granitic relics, while only 15% of the authigenic Ca released by weathering is reincorporated in the calcite. This suggests that 373 kg/m^2 of calcium (i.e., three times the original amount) is imported into the calcrete from allochtonous sources, probably due to aeolian transport from distant limestone formations. © 2000 Elsevier Science B.V. All rights reserved.

Keywords: Calcrete; Mass-balance; Calcium; Iso-volume; Chemical weathering; Granite; Toledo, Central Spain, Europe

1. Introduction

Calcretes are thick carbonate crusts of pedogenic origin developed at or near the soil surface. They result from the net and relative accumulation of

---

[*] Corresponding author. Tel.: +33-4-42-97-15-38; fax: +33-4-42-97-15-40.

E-mail addresses: achiquet@cerege.fr (A. Chiquet), colin@cerege.fr (F. Colin), hamelin@cerege.fr (B. Hamelin), michard@cerege.fr (A. Michard), nahon@cerege.fr (D. Nahon).

0009-2541/00/$ - see front matter © 2000 Elsevier Science B.V. All rights reserved.
PII: S0009-2541(99)00240-5

calcium in soils under arid and semi-arid climates with a marked dry season.

Calcrete genesis is driven by alternating wet and dry seasons (Wang et al., 1994) that produce the geochemical conditions of a thermodynamic disequilibrium for primary silicate minerals, which are then replaced by calcium carbonate (Nagtegaal, 1969; Aristarain, 1971; Boulet, 1974; Chapman, 1974; Nahon, 1976; Nahon et al., 1975; Millot et al., 1977; Durand, 1979; Bech et al., 1980; Reheis, 1988; Ducloux et al., 1990; Monger and Daugherty, 1991a,b). The process of calcite accumulation in soils has been simulated with box models (McFadden and Tinsley, 1985; Marion et al., 1985; Mayer et al., 1988). However, only a few studies have attempted to quantify the elemental mass transfer subsequent to the development of calcrete in soils, in spite of the recent development of the mass-balance calculation methods in weathering systems (Millot and Bonifas, 1955; Nesbitt and Wilson, 1992; Nesbitt et al., 1980; Brimhall et al., 1991, 1992; Colin et al., 1992; Nahon and Merino, 1997).

The purpose of our work is to quantify the losses and gains of chemical elements resulting from in situ weathering and calcitization of a granitic bedrock. Iso-volumetric mass-balance calculations are applied in order to model the chemical dynamics of these particular weathering conditions under arid climates. The chosen study area is the calcrete-rich plateau of Toledo, Central Spain (39°42′N, 4°18′W, 725 m) (Fig. 1), where the present-day regional climate is semi-arid, with a mean annual rainfall of 370 mm and a mean annual temperature of 14.7°C. Evaporative conditions characterize the dry hot season between May and September. The main bedrock formations of the plateau are granite, migmatite and gneiss from the Hercynian orogeny. Quartzite and greenschist are found in the surrounding relief making up

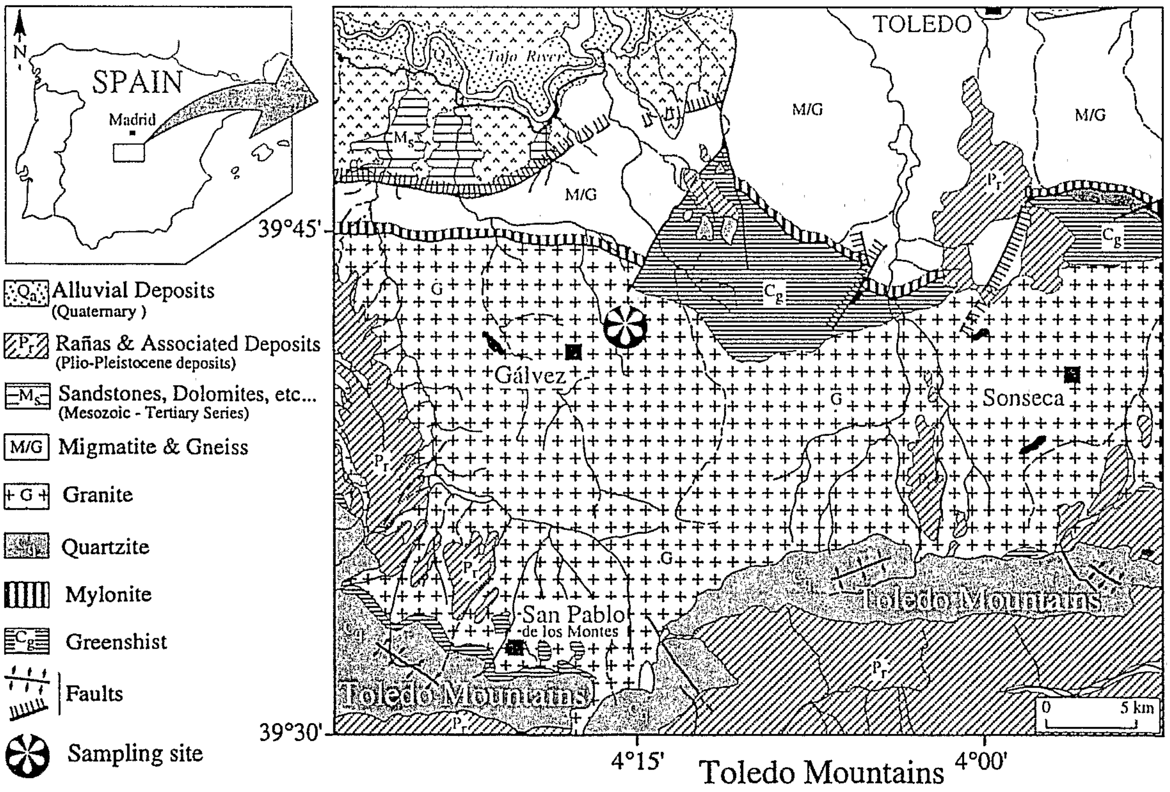

Fig. 1. Geological map of the studied area, showing the major units of granite, migmatite and gneiss substratum, on the plateau located between the Toledo Mountains (greenschists and quartzites) to the south, and the Tajo river valley to the north and the west.

the Toledo Mountains and some scattered inselbergs (Fig. 1). No limestone formations are found locally, except for some remnants of marine Mesozoic–Tertiary sediments on the northern and eastern edges of the Toledo platform.

From the middle Miocene to the lower Pleistocene, the deep Hercynian basement was locally buried under an alluvial sedimentary cover termed ''Ranas'' (Vicente et al., 1991, 1997). Since then, present-day rivers and arroyos have eroded this alluvial cover, allowing the weathering front to crop out underneath. We investigated a calcrete profile developed on granitic bedrock, at a site where the weathering mantle is presently about 7 m thick.

2. Sampling and experimental methods

Samples of fresh and weathered rocks were collected from a typical profile in a recent quarry (Fig. 1). A Sr isotopic study of this profile is reported in a companion paper (Chiquet et al., 1999). A general description of the different layers is shown in Fig. 2. Two types of samples were taken: (1) undisturbed samples were collected in oriented plastic boxes for petrographic observations; and (2) powdered samples (0.5 to 2 kg) were collected at the same place in plastic bags (2 l). A 5-kg block of fresh granite was collected from a nearby outcrop, about 800 m from the studied profile.

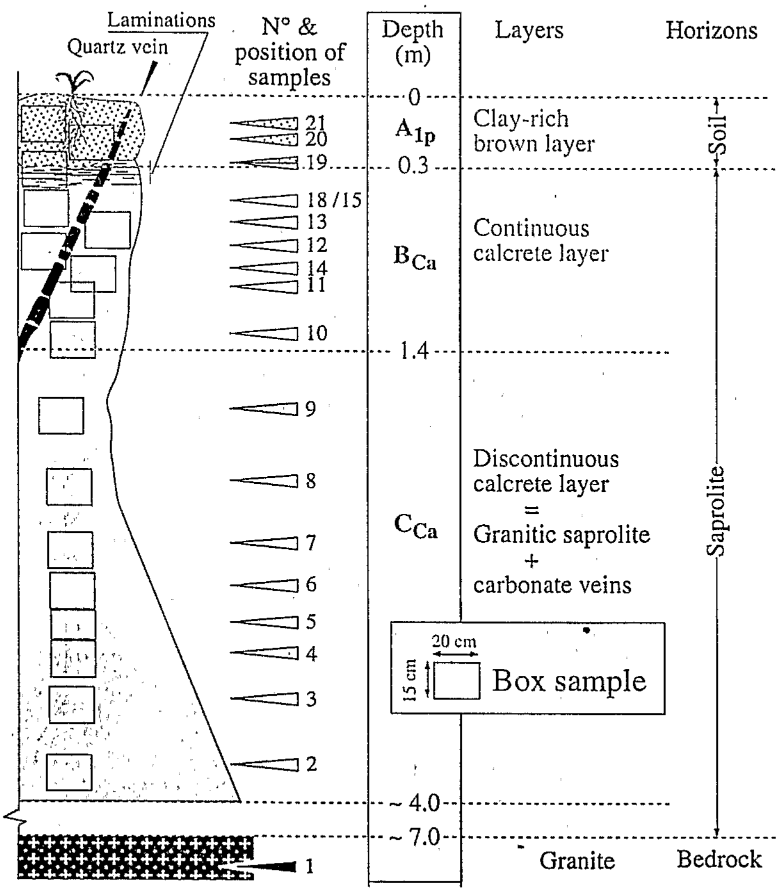

Fig. 2. Arrangement of the calcic horizons in the Gálvez calcrete. Initial quartz veins and fractures cross-cut the saprolite and the calcrete without any structural perturbation. Samples collected in plastic bags (arrows) represent a mass ranging from 0.5 to 2 kg. Undisturbed samples for thin sections have been collected in plastic boxes of ~ 3 dm^3.

Major and trace element analyses were determined by ICP-AES. The samples were dried at 60°C and totally dissolved with concentrated $HF/HClO_4/HNO_3$. Bulk density (ρ_w) measurements were performed on ~10-ml samples after drying by immersion in water after coating with molten paraffin wax, in order to measure the displaced volume. The uncertainty resulting from this procedure is about 3%. Grain density (ρ_g) was measured on powdered samples (30 μm) with an air pycnometer, with a mean error of 2%. Porosity (ϕ) was calculated as:

$$\phi = 1 - \rho_w/\rho_g \quad (1)$$

Five replicates were systematically measured, indicating a reproducibility of 6% (2σ).

Thin sections were prepared from oriented samples after induration with epoxy resin. The calcium-carbonate concentration was determined by calcimetry on powdered samples, calibrated on a pure calcium carbonate sample (reproducibility of 5%).

Mass-balance calculations developed in this paper are based on the general Eq. (2) used by Brimhall and Dietrich (1987), Brimhall et al. (1991, 1992) and Colin et al. (1992, 1993). The transport factor $\tau_{j,w}$ of an element j in the weathered material is defined as:

$$\tau_{j,w} = \left[\left(\frac{C_{j,w}}{C_{j,p}}\frac{\rho_w}{\rho_p}\right)(\varepsilon_{i,w}+1)\right] - 1 \quad (2)$$

where i is an element considered as immobile and j a chemically mobile element during weathering, ρ is the bulk density (in g/cm^3), C is the concentration (wt.%), and "w" and "p" refer to the weathered rock and the fresh rock, respectively. $\varepsilon_{i,w}$ (3) is the volumetric factor defined as:

$$\varepsilon_{i,w} = \left(\frac{C_{i,p}}{C_{i,w}}\frac{\rho_p}{\rho_w}\right) - 1 \quad (3)$$

where $\varepsilon_{i,w} < 0$ for collapse, $\varepsilon_{i,w} > 0$ for expansion and $\varepsilon_{i,w} = 0$ for iso-volumetric weathering. $\tau_{j,w}$ reflects the gain or loss of element j in the weathered rock compared to the parent rock ($-1 = \tau_{j,w} = +1$; $\tau_{j,w} = 0$ for loss and $\tau_{j,w} = 0$ for gain).

3. Results

3.1. Field observations

Calcareous soils are widespread on all the lithologies of the dissected plateau, except on the inselbergs (Vaudour, 1979). Carbonate accumulation is related to elevation and, thus, to local average rainfall: there are no carbonate accumulations or calcareous soils in the Toledo Mountains above 800–900 m elevation, where sub-humid conditions prevail, which prevent carbonate precipitation.

In typical profiles, calcite occurs as powdery or indurated layers; the thickness of the calcrete horizons ranges from 10 cm up to 4 m. The carbonates are intermingled with weathered remnants of the host parent materials. No carbonate-rich layers were ob-

Fig. 3. (a) Mineralogical assemblage of the parent granite (Gálvez, 30 km southwest of Toledo, Central Spain). The rock is made up of quartz (Q), plagioclase (P), K-feldspar (F), and biotite (B). Crossed polars. (b) Zircon extracted from the fresh rock. No dissolution features (e.g., rounded edges and corners) are identified. (c) Early stage of a pseudomorphic replacement of the granite by clays. 3.50 m depth in the profile: plagioclase grain (P) is partly replaced by a green secondary clay aggregate (Sc). Plagioclase fragments are in optical continuity. Toward top left and right, biotites (B) are bleached and secondary clays (Sc) are also developed between their layers. Crossed polars. (d) Dissolution etch pits (arrows) and rounded edges and corners of zircon grain in the saprolite (continuous calcrete layer: 1.20 m depth). All zircon grains extracted from the calcrete layers (continuous or discontinuous) exhibit small to large dissolution features ranging from simple etch pit to rounded corners. (e) Higher in the profile (2.10 m depth), calcite (C) appears beside secondary clays (Sc). Detail of the replacement of the weathering products of the granite (secondary clays: Sc) by sparry and micritic calcite (C) along voids. Crossed polars. (f) Top part of the calcrete (continuous calcrete layer: 0.5 m depth). A K-feldspar (Fk) is "directly" replaced by calcite (Cc). The different relics of the K-feldspar (dark) have kept their original orientation. Crossed polars. (g) Other exemple of "direct" replacement of a primary mineral (microcline: M) by calcite (0.40 m depth). No displacement is observed: all fragments are in optical continuity. This pseudomorphic replacement by calcite (C) has preserved the original cleavage of the microcline (arrows). Crossed polars. (h) Detail of the top of the continuous calcrete profile. Relics of granite are scattered in the massive calcitic matrix (C). The sides of the relics show numerous corrosion features. A K-feldspar (F; bottom left) is partly invaded by calcite: not replaced portions are undisplaced. Crossed polars. Photomicrographs were taken by A. Chiquet.

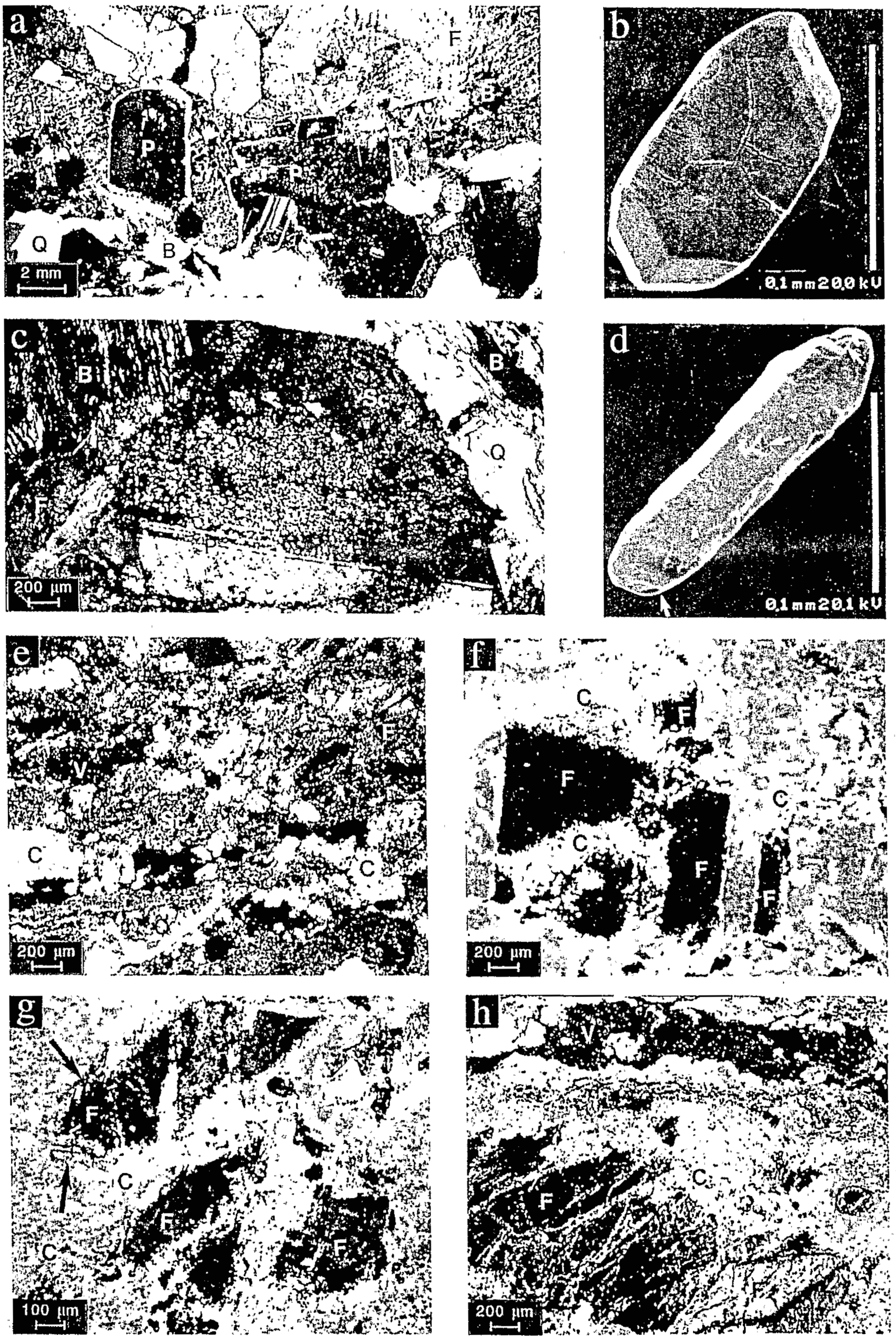
a
F
B
P
P
Q
B
2 mm
b
0.1 mm 20.0 kV
c
B
B
Sc
Q
F
200 µm
d
0.1 mm 20.1 kV
e
V
F
Sc
C
C
200 µm
f
C
F
F
C
C
F
F
200 µm
g
F
C
C
F
F
100 µm
h
V
C
F
200 µm

served within the valleys, where only ball-shape residues of parent rock are left over by weathering and erosion processes. Ephemeral stream-waters run along these valleys, directly on the granite.

A typical calcrete profile was selected on granitic basement (Fig. 1), at an elevation of 720 m. From top to bottom, the profile is arranged into three main units (Fig. 2): (1) the fresh bedrock (a biotite granite with perthitic phenocrysts), at about 7 m below surface; (2) a granitic saprolite (~ 7.0 to 0.3 m); and (3) a topsoil (0.3 m to the surface). The following three zones can be distinguished within the saprolite (Fig. 2).

(1) A massive weathered granite, below 3.7 m, with very minor calcite veins.

(2) A discontinuous calcrete layer (C_{Ca}, from 3.7 to 1.4 m): white calcite-rich domains appear all along the main fractures of the saprolite, and develop progressively upward. The network of calcitic veins is in conformity with the preserved fracturing of the weathered granite.

(3) A continuous calcrete layer (B_{Ca}, from 1.4 to 0.3 m): calcite (white with reddish zones at the top of the profile) forms a continuous matrix enclosing rounded relics of weathered granite and smectites. The whole layer still preserves the texture of the fresh parent granite. XRD analysis performed on the carbonate show that it is a low-magnesium calcite (Mg < 5%).

The topsoil (A_{1p}) consists of a 0.3-m-thick clay-rich brown layer overlying the continuous calcrete. It is mainly composed of primary relics (quartz, K-feldspar, plagioclase) and smectite. The concentration of organic matter remains low (0.45% to 0.53% of organic C) except for scattered roots.

3.2. Microscope examination

In order to specify the relationships between calcitization and weathering, as well as the subsequent chemical paths, petrographic and petrological observations were performed on thin sections. The main results are the following.

(1) The parent granite has a mineralogical composition dominated by quartz (42%) with mica (13%), plagioclase (27%) and perthitic K-feldspar phenocrysts (18%) (Fig. 3a). The chemical composition of plagioclase ranges from calcic to more sodic with normal zonation. Micro-cracks and fractures indiscriminately cross-cut all minerals.

(2) The micro- and macro-crack network present in the fresh rock is undisturbed all along the saprolite. Moreover, plagioclases, generally with a Ca-rich core, are pseudomorphically replaced by clays (Fig. 3c). Biotites (main mica phase) exhibit similar weathering, starting by bleaching (loss of iron), expansion of the layers, and neoformation of brown to green clays. X-ray diffraction analysis of the ≤ 2 μm fraction of the saprolite indicates the high abundance of smectite. K-feldspar is relatively well preserved compared to plagioclase. No phase displacements are observed, even if some micro-fractures (< 50 μm) are infilled by secondary clays.

(3) Above 3.7 m, we observe the first millimeter-scale veins of white calcite controlled by the initial fracturing of the rock. In the first calcitic stages, secondary clays are replaced by small amounts of calcite along microfractures (Fig. 3e). These fractures, which are filled with carbonate, become more numerous and widen upward in the profile, until they form a connected calcareous network. The calcitization increases upward in the saprolite, with a progressive decrease of the tiny relics of primary minerals within the veins. These relics have clearly remained in place within the rock structure. The walls of the calcitic veins are asymmetric, which indicates that the calcitization process results from a pseudomorphic replacement of primary mineral phases.

(4) From 1.4 to 0.3 m, the micritic calcite-rich matrix englobes remnants of saprolitic material, where plagioclase and biotite are increasingly weathered to clays. In the most carbonated zones, pseudomorphic replacement of primary minerals by calcite is almost complete (Fig. 3f,g,h). The porous micritic matrix shows evident features of recrystallisation such as sparite, micro-sparite and needle crystals observed in voids. Some calcitic domains exhibit a brown colour and a low porosity. Calcitized roots and pseudo-mycelia have also been identified.

Evidence of biological activity (roots, filamentous algae, etc.) are noticed both in the B_{Ca} and the C_{Ca} layers. According to Milnes (1992) and Wright et al. (1995), organic processes may directly or indirectly cause the precipitation of calcite. The development of various calcitic habits (i.e., needles) might be

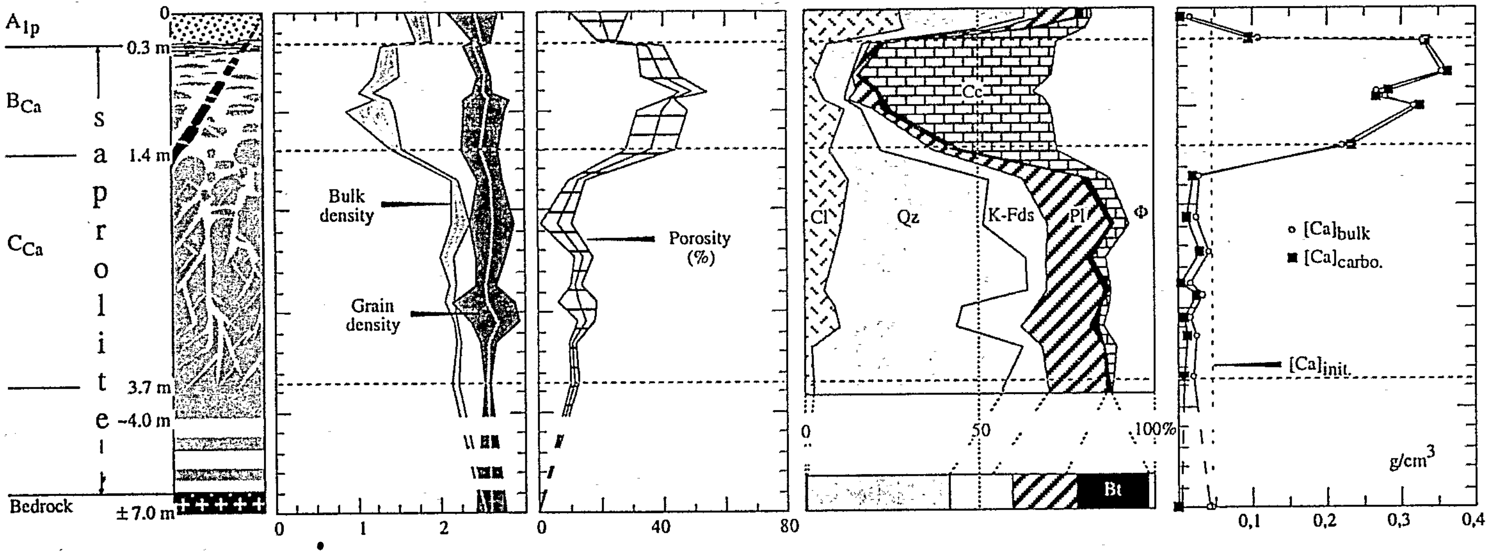

Fig. 4. Depth profiles of bulk and grain densities, porosity (calculated from density measurements); mineralogical composition; calcium concentration in the granite ($[Ca]_{init}$), bulk calcium concentration ($[Ca]_{bulk}$) and calcium carbonate content ($[Ca]_{carbo}$). The mineralogical distribution his calculated from X-ray diffraction data (vol.%) and includes the bulk porosity (Φ). Cl: clay fraction; Qz: quartz; K-Fd: K-feldspar; Pl: plagioclase; Bt: biotite; Cc: calcite, Φ: bulk porosity.

Table 1

Chemical composition (Cc) and Transport function ($\tau_{j,\mathrm{w}}$) for samples from the profile. For the major elements, the Cc is in weight percent, while for trace element, Cc is in micrograms per gram. All granite $\tau_{j,\mathrm{w}}$ values are equal to zero because granite is assumed to be the reference (five aliquots)

No.	(1)	Depth (cm)	ρ	SiO_2		Al_2O_3		Fe_2O_3		TiO_2	
				Cc	$\tau_{j,\mathrm{w}}$	Cc	$\tau_{j,\mathrm{w}}$	Cc	$\tau_{j,\mathrm{w}}$	Cc	$\tau_{j,\mathrm{w}}$
21-95	A_{1p}	10	1.87	56.9	−0.39	18.1	−0.21	5.33	0.05	0.38	−0.45
20-95	A_{1p}	30	1.90	52.9	−0.42	14.8	−0.34	3.84	−0.23	0.29	−0.58
19-95	B_{Ca}	35	1.48	25	−0.79	8.2	−0.71	2.31	−0.64	0.19	−0.78
15-95	B_{Ca}	65	1.51	28	−0.76	5.37	−0.81	1.37	−0.78	0.12	−0.86
12-95	B_{Ca}	83	1.22	31.1	−0.78	6.43	−0.82	1.46	−0.81	0.16	−0.85
14-95	B_{Ca}	90	1.40	33.9	−0.73	7.22	−0.76	1.41	−0.79	0.19	−0.80
11-95	B_{Ca}	100	1.46	31.3	−0.74	6.54	−0.77	1.24	−0.81	0.15	−0.83
10-95	B_{Ca}	140	1.55	45.9	−0.59	8.85	−0.68	1.75	−0.71	0.24	−0.71
9-95	C_{Ca}	170	2.23	67.5	−0.13	14.5	−0.24	2.97	−0.30	0.42	−0.28
8-95	C_{Ca}	213	2.44	67.7	−0.05	15.1	−0.13	2.81	−0.28	0.39	−0.27
7-95	C_{Ca}	245	2.17	66.2	−0.17	14.1	−0.28	2.79	−0.36	0.38	−0.36
6-95	C_{Ca}	275	2.19	68.6	−0.13	15.1	−0.22	2.78	−0.36	0.38	−0.36
5-95	C_{Ca}	290	2.18	66.6	−0.16	14.6	−0.25	2.86	−0.34	0.39	−0.35
4-95	C_{Ca}	310	2.20	68.2	−0.13	14.8	−0.23	2.84	−0.34	0.39	−0.34
3-95	C_{Ca}	330	2.25	67	−0.13	14.6	−0.23	2.75	−0.34	0.38	−0.34
2-95	C_{Ca}	370	2.21	68.8	−0.12	14.9	−0.23	2.5	−0.41	0.34	−0.42
1-95	Granite	700	2.60	66.2	0	15	0	3.63	0	0.5	0
2σ	–	–	0.06	2.06	0.02	0.25	0.01	0.16	0.02	0.03	0.03

favoured in pores where humid conditions are preserved even during the dry season.

(5) In the transition between the B_{Ca} and A_{1p} layers, plurimillimetric rounded calcitic zones persist with a clay-rich reddish matrix. Horizontal laminations are observed, which are made up of alternating calcitic and organic/clay beds.

(6) In the upper 30 cm, gravelly relics of the saprolite are coated by Fe-rich clays and iron oxides. There is no calcite in the topmost 25 cm of the soil, which are clearly bioturbated by the root activity.

3.3. *Iso-volume mass-balance calculations*

Bulk and grain densities, porosity values, mineralogical composition and calcium contents (granite, bulk and carbonate) are reported in Fig. 4; Table 1 gives the chemical composition of each sample.

In order to calculate the mass transfer of weathering products and the calcium fluxes within the calcrete profile, an appropriate frame of reference must be selected. Macroscopic (Fig. 2) and microscopic observations (Fig. 3a,c,e,f,g,h) show that (1) the weathering process has preserved the initial volume of the parent rock throughout the saprolite, and (2) the calcitization also takes place without disturbing the original bulk volume of the host material. The process of pseudomorphic replacement of primary phases by calcium carbonate is well accepted, based on numerous conclusive microscopic observations reported in the literature (Aristarain, 1971; Chapman, 1974; Nahon, 1976, 1991; Nahon et al., 1975; Millot et al., 1977; Reheis, 1988; Monger and Daugherty, 1991a,b). The mass-transfer budget during calcrete development must, therefore, be calculated on a constant-volume assumption, following Millot and Bonifas (1955), Trescases (1975), Gardner (1980) and Gardner et al. (1978). Chemical imports and exports must be referred to a given parent-rock volume, which is conservative during both weathering and calcitization. Thus, $\varepsilon_{i,\mathrm{w}}$ is equal to zero in Eq. (2), and the transport factor $\tau_{j,\mathrm{w}}$ is expressed as (4):

$$\tau_{j,\mathrm{w}} = \frac{\rho_{\mathrm{w}} C_{j,\mathrm{w}}}{\rho_{\mathrm{p}} C_{j,\mathrm{p}}} - 1 \tag{4}$$

CaO		MgO		Na_2O		K_2O		Rb		Sr		Zr		Th	
Cc	$\tau_{j,w}$	Cc	$\tau_{j,w}$	Cc	$\tau_{j,w}$	Cc	$\tau_{j,w}$	Cc	$\tau_{j,w}$	Cc	$\tau_{j,w}$	Cc	$\tau_{j,w}$	Cc	$\tau_{j,w}$
1.26	−0.63	1.4	−0.15	1.18	−0.76	3.29	0.01	190	0.01	70	−0.65	90	−0.60	12	−0.34
8.07	1.42	1.3	−0.17	1.13	−0.76	3.53	−0.44	200	−0.33	90	−0.55	70	−0.68	8	−0.55
31.1	6.28	0.9	−0.57	0.78	−0.87	1.53	−0.39	95	−0.28	200	−0.21	50	−0.82	5	−0.78
32.8	6.78	1	−0.53	0.55	−0.91	1.25	−0.79	70	−0.73	190	−0.24	40	−0.86	1	−0.96
30.5	4.85	0.8	−0.68	1.03	−0.86	1.55	−0.83	100	−0.80	280	−0.29	40	−0.83	1	−0.88
27.7	5.12	0.8	−0.62	1.43	−0.78	2.4	−0.83	80	−0.81	220	0.04	50	−0.88	3	−0.96
30.3	5.96	0.9	−0.57	0.93	−0.85	1.87	−0.69	100	−0.73	370	0.43	50	−0.82	1	−0.96
20	3.89	1.1	−0.46	1.73	−0.71	2.64	−0.75	120	−0.72	350	0.44	80	−0.70	4	−0.82
1.79	−0.37	1.2	−0.08	2.93	−0.28	4.29	−0.63	190	−0.65	120	−0.29	130	−0.30	10	−0.34
1.43	−0.45	1.2	−0.06	2.87	−0.23	4.62	−0.13	210	−0.20	160	0.03	120	−0.30	11	−0.21
2.65	−0.09	1.2	−0.12	2.66	−0.36	4.18	0.02	185	−0.03	150	−0.14	120	−0.37	11	−0.29
1.07	−0.63	1.2	−0.10	2.72	−0.35	4.39	−0.18	190	−0.24	140	−0.19	120	−0.37	10	−0.35
2.15	−0.26	1.2	−0.14	2.89	−0.31	4.33	−0.13	190	−0.21	140	−0.19	120	−0.37	10	−0.36
1.05	−0.64	1.1	−0.17	3.06	−0.26	4.42	−0.15	205	−0.22	150	−0.12	130	−0.31	10	−0.35
1.6	−0.43	1.2	−0.09	2.73	−0.32	4.31	−0.12	190	−0.14	140	−0.16	120	−0.35	10	−0.33
1.21	−0.58	1.1	−0.22	3.37	−0.18	4.48	−0.12	195	−0.19	140	−0.18	110	−0.41	9	−0.41
2.42	0	1.2	0	3.5	0	4.27	0	203	0	144	0	154	0.00	13	0.00
0.09	0.02	0	0.01	0.04	0.01	0.1	0.01	4.5	0.01	8.9	0.03	4.2	0.03	0	0.01

The mass-transfer budget Δm_j (kg/m^3) of a chemically mobile element "j", is given by (5):

$$\Delta m_j = \tau_{j,w} \rho_p C_{j,p} \quad (5)$$

The flux of mass exportation $M_{j,w}$ (kg/m^2) for the weathering system can be approached by integrating the mass-transfer budget between given depths z_i and z_f:

$$M_{j,w} = \int_{z_f}^{z_i} \tau_{j,w} \rho_p C_{j,p} \, dz \quad (6)$$

The chemical budgets have been calculated for major and trace elements (Th, Zr, Rb and Sr). The transport factors ($\tau_{j,w}$) are listed in Table 1 and plotted in Fig. 5. All the elements are depleted in various proportions in the C_{Ca} layer. In the discontinuous calcrete layer (C_{Ca}), the average transport factors decrease from values of −0.11 to −0.43, along the series K, Mg, Si, Sr, P, Rb, Al, Na, Th, Ti, Fe, Zr, Mn and Ca. In the continuous calcrete layer (B_{Ca}), the massive calcitization gives a positive transport factor for Ca (+5.48) and Sr (+0.03), while all other elements are largely depleted (−0.57 to −0.87).

According to Eq. (6), we can calculate the flux of each element from the profile. By summing all the elements, we have a direct access to the global flux of mass exportation. We calculate that 750 kg/m^2 of major cations have been exported out of the continuous calcrete layer (0.3 to 1.4 m), 575 kg/m^2 from the discontinuous calcrete layer (1.4–3.7 m), and 380 kg/m^2 from the granitic saprolite (free of carbonates) between 3.7 and 7.0 m. In weight percent, the flux of exportation from the profile is controlled by Si (64% of the global flux), Al (23%), Fe (9%), Na (8%), K (7%), Mg (1%) and Ti (1%). By comparison, 275 kg/m^2 of Ca and 30 g of Sr have been imported in the continuous calcrete layer while 15 kg/m^2 of Ca and 90 g/m^2 of Sr have been lost from the discontinuous calcrete layer.

The global inventory of calcium carbonate estimated from calcimetric measurements, is 975 kg/m^2 (390 kg/m^2 of Ca). 85% is accumulated in the continuous calcrete layer (325 kg/m^2) and 15% in the discontinuous calcrete layer (65 kg/m^2).

4. Discussion

Schematically, the genesis of the calcrete profile can be analysed as a two-stage process: (1) weather-

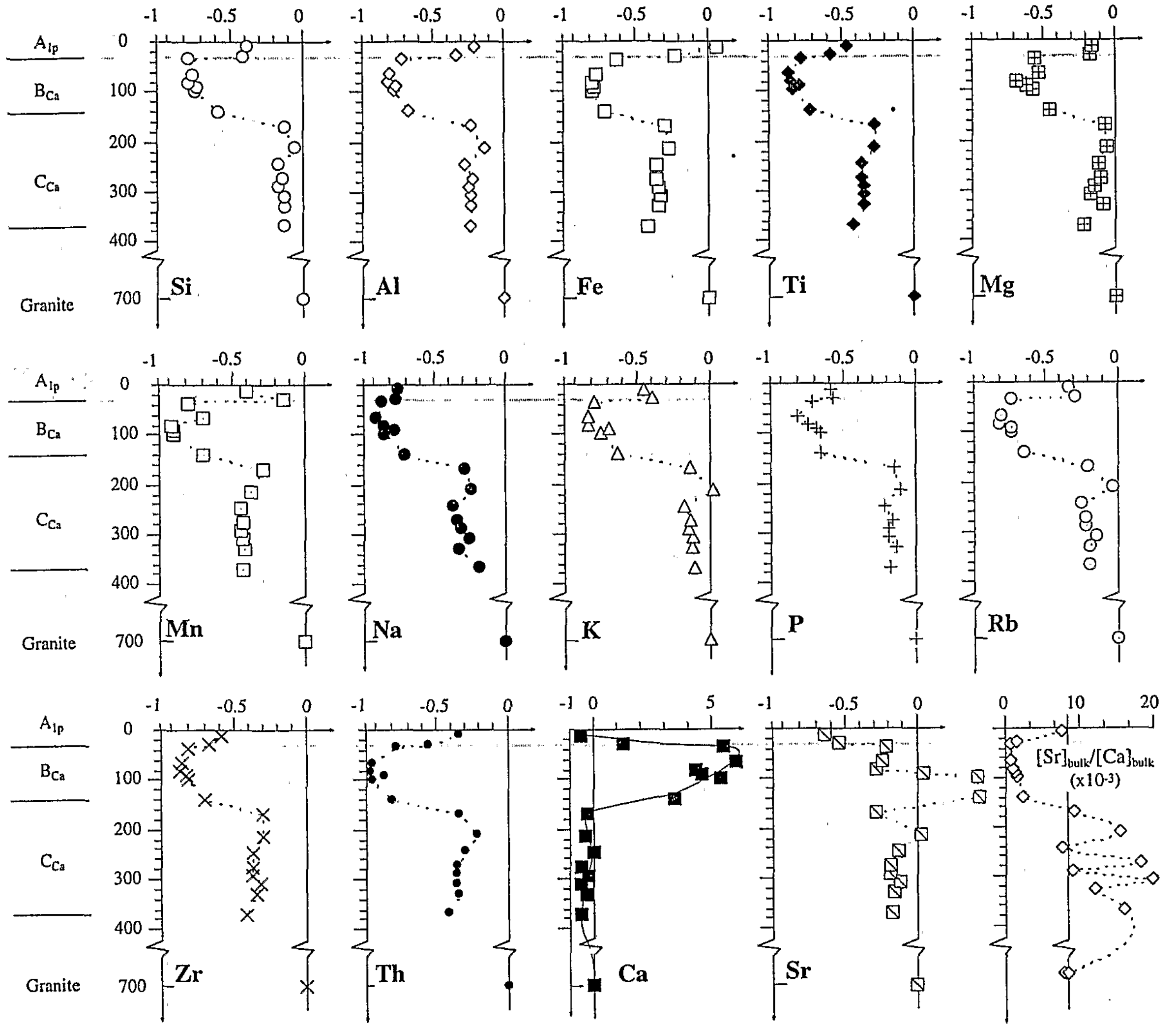

Fig. 5. Transport factor (τ) of major and some trace elements (Rb, Sr, Zr, Th) of the calcrete profile. The $[Sr]_{bulk}/[Ca]_{bulk}(\times 10^{-3})$ is also plotted. A general depletion is observed for all element except for Ca and Sr in the B_{Ca} layer. In the A_{lp} layer, losses are less important than in the B_{Ca} layer while a gain of Fe is observed. The loss of Fe in the C_{Ca} layer represent 35% of the initial content (granite).

ing of the fresh granite, followed by (2) progressive calcitization of the saprolite. In the case of the Montes de Toledo area, it is difficult to elucidate completely the exact relationship between the two processes and their respective timing, due to the ubiquitous occurrence of paleoweathering facies developed on different lithologies in this area (Vicente et al., 1997). However, the upper kaolinitic unit described by Vicente et al. (1997) in other paleoweathering profiles is completely absent from the site studied here. On the other hand, the mineralogical evidence presented above demonstrates active pseudomorphic replacement of the silicate minerals by calcite (Fig. 3). Therefore, calcitization and weathering of the granite must be considered as synchronous and interrelated as proposed by Wang et al. (1994).

Pseudomorphic replacement of silicate minerals by calcite requires specific geochemical conditions, resulting in simultaneous removal of large amounts

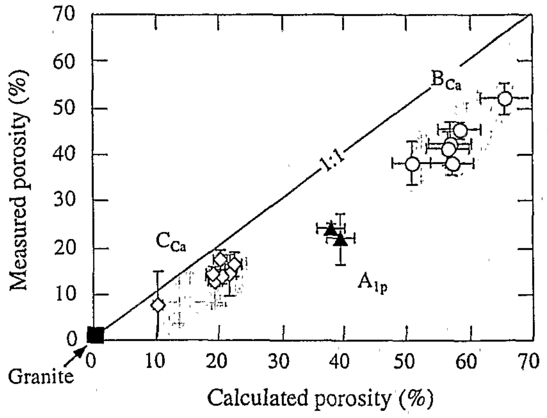

Fig. 6. Measured porosity vs. calculated porosity for each sample of the studied profile. Measured porosity is obtained from density measurements. The calculated porosity takes into account the volume created by the loss of major chemical elements during weathering of the parent rock. It is obtained by summing all the fluxes of mass exportation, taking into account the contribution of structural oxygen (49 wt.% in the fresh rock). The initial parent rock porosity is about 1%. In the discontinuous calcrete layer (C_{Ca}), voids are associated with the weathering of primary minerals such as plagioclase and mica, and result from the exportation of weathering products. In the continuous calcrete layer (B_{Ca}), the microporosity is more structural, and localised in a micritic crystalline-plasma.

of silica and neoformation of calcium carbonate. Wang et al. (1994) proposed that the replacement process is directly related to the seasonal alternation of wet and dry periods. During dry seasons, evaporation induces calcium carbonate and smectite precipitation in the pores (Fig. 3e). This neoformation of secondary clays depletes dissolved silica from the soil solutions (Paquet, 1983, 1993), inducing further dissolution of parent silicates (Merino et al., 1993). In the following wet season, smectite dissolves faster than calcium carbonate, due to the alkaline conditions (pH values often higher than 9; Ruellan, 1971; Nahon, 1991). Silicon and other cations are, thus, flushed away by circulating soil-waters, leaving empty space for further calcium carbonate precipitation during the next dry season. Repetition of this seasonal cycle results in concomitant silicate removal and $CaCO_3$ accumulation.

This model does not preclude that some of the smectites may have been inherited from previous weathering stages. Incipient stages of calcrete precipitation may even be favoured on lithologies that have been previously weathered, i.e., with higher porosity and higher smectite content. Nevertheless, the chemical budgets discussed here are calculated with respect to the original unweathered granite, and, thus, do not depend on any assumption regarding this initial stage of alteration before calcrete initiation.

The chemical budget of the calcitization process is reflected in the net loss of matter from the profile, as calculated above (1325 kg/m^2). This implies the development of voids, since the initial volume of the parent rock is preserved and no collapse is observed. Corroboration of our mass-balance calculation is obtained by plotting the measured porosity data vs. the calculated values of porosity for each sample (Fig. 6). Measured porosity is about 25% lower than that predicted from the budget calculation in the clay-rich brown layer (A_{1p}) and in the continuous calcrete layer (B_{Ca}). This is probably due to the persistence of a closed residual microporosity (< 30 μm) in the calcite and in the fine clay fraction, as demonstrated by Dekayir (1994) from Hg porosimetry.

4.1. Weathering of the granite and saprolite formation

The global chemical depletion of the saprolite compared to the fresh rock is due to specific cation losses (Table 1; Fig. 5). In the saprolite, Ca, Fe and Na are the main cations exported from the weathered granite. By comparison, K, Si and Mg exhibit relatively lower rates of exportation (Table 2). Petrographic observations indicate that plagioclase and biotite are weathered to clays, releasing a significant amount of Ca, Sr, Na and Fe into solution (Nesbitt, 1979; Nesbitt et al., 1980), while Si, Al, Mg precipitate in situ within smectites. The perthitic phe-

Table 2
Exportation of chemical element (%) between the weathered granite and the fresh rock
Concentrations of the element j in the weathered granite is obtained from those of the discontinuous calcrete layer ($n = 8$ samples) after correction from the contribution of Ca and Sr of calcitic veins, in order to evaluate the non-calcareous weathering of the parental rock

Element j	Ca	Mn	Fe	Ti	Th	Zr	Na	Al	Sr	Rb	P	Mg	Si	K
$X_{j,\mathrm{weathering}}$	42	41	34	34	33	32	29	22	20	18	16	13	13	12
±	5	5	4	5	4	5	6	2	8	5	3	5	2	4

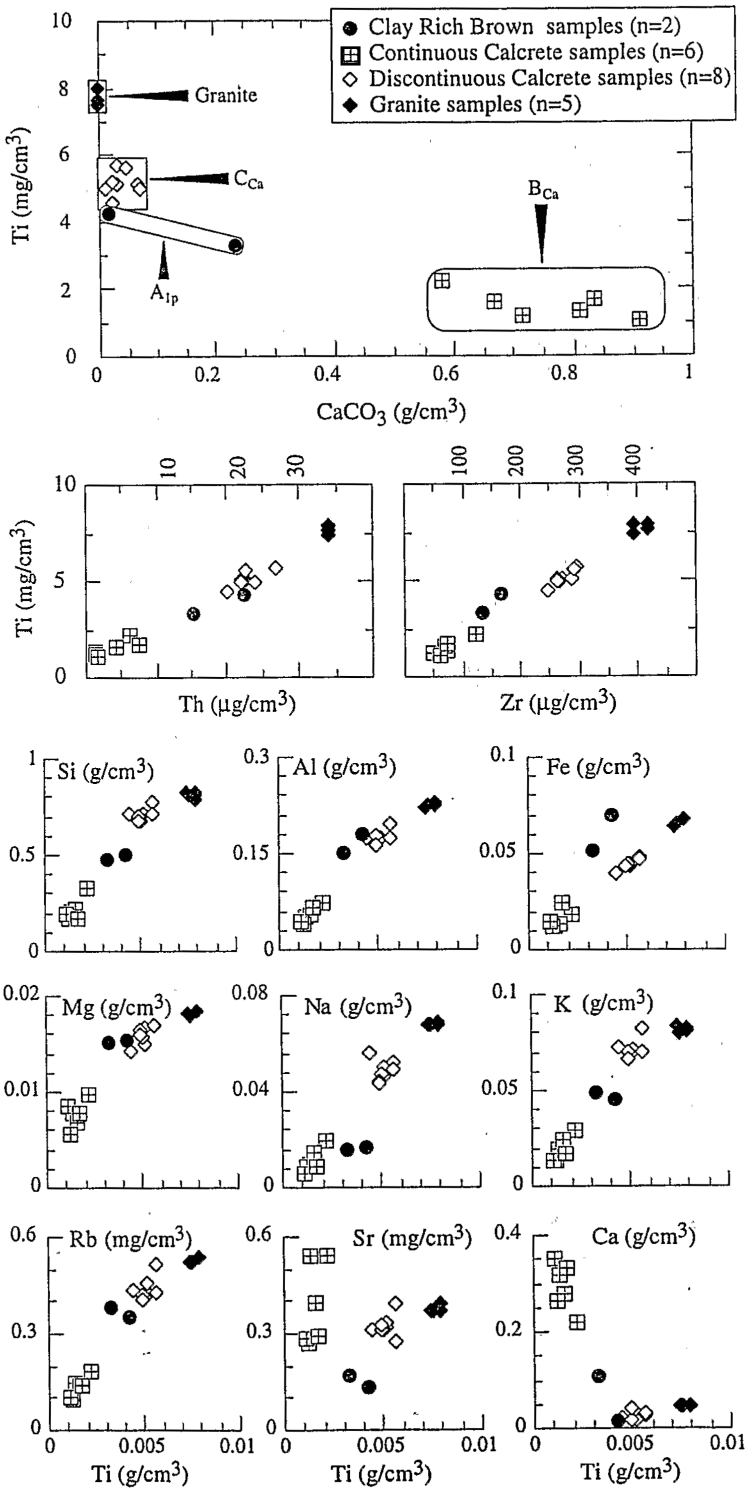
● Clay Rich Brown samples (n=2)
⊞ Continuous Calcrete samples (n=6)
◇ Discontinuous Calcrete samples (n=8)
◆ Granite samples (n=5)
Granite
C_Ca
B_Ca
A_1p
Ti (mg/cm³)
CaCO₃ (g/cm³)
0
0.2
0.4
0.6
0.8
1
2
4
6
8
10
5
Th (µg/cm³)
Zr (µg/cm³)
10
20
30
100
200
300
400
Si (g/cm³)
Al (g/cm³)
Fe (g/cm³)
Mg (g/cm³)
Na (g/cm³)
K (g/cm³)
Rb (mg/cm³)
Sr (mg/cm³)
Ca (g/cm³)
0.5
0.3
0.15
0.1
0.05
0.02
0.01
0.08
0.04
0.6
0.4
0.2
0.005
Ti (g/cm³)

nocrysts of K-feldspar are relatively well preserved, contributing to the partial conservation of K and Rb.

Laboratory experiments and Sr isotopic studies have demonstrated the slower weathering rate of K-feldspar compared to that of plagioclase (Lasaga, 1984; Blum et al., 1994; Blum and Erel 1995, 1997; White et al., 1996; Chiquet et al., 1997). Blum et al. (1994, 1997) have also shown that biotite weathers four to eight times faster than plagioclase, although other studies have recently shown that biotite can weather more slowly than plagioclase in some occurrences under tropical climates (Murphy et al., 1998). Moreover, biotite weathering involves the formation of secondary clays (smectite or vermiculite), which proceeds by oxidation of Fe^{2+} to Fe^{3+} accompanied by an absolute loss of Fe, depletion of K^+ from interlayer sites, and partial retention of Mg^{2+}. Other minor interlayer cations such as Ca^{2+} and Sr^{2+} are also lost during this transformation (Velbel, 1985; Drever and Hurcomb, 1986). However, part of the K^+ extracted from the biotites is probably reincorporated into smectites resulting from weathering of the plagioclase, while Na^+, Ca^{2+} and Sr^{2+} are released.

In the studied calcrete, Ti, Zr and Th concentrations are closely correlated to each other, and show a large decrease with increasing calcium carbonate concentration (Fig. 7). For instance, the iso-volumetric budget calculation indicates that Zr is depleted by 80% in the continuous calcrete and by 35% in the discontinuous calcrete, compared to the fresh rock (Fig. 8). These three elements, which are generally considered as immobile during weathering, are even more depleted than Mg, K, Si and Al in the saprolite (discontinuous calcrete). Such a large depletion might be suspected to result from lateral heterogeneities of the parent granite, but since the fresh rock could not be sampled directly beneath the calcrete profile itself, we suggest that this may also reflect enhanced alteration processes of accessory minerals under the highly alkaline conditions of calcrete formation. SEM mapping shows that, in the fresh rock, Zr (154 ppm) is associated with autochtonous euhedral micrometric zircons included in biotites. SEM observations of zircon grains extracted from the saprolite and the carbonate layer show clear corrosion features compared to the unweathered zircons from the fresh rock (Fig. 3b,d). Other examples of Zr (Melfi et al., 1996; Nahon and Merino, 1996) and Ti mobility (Gardner, 1980) have been reported previously in some saprolites, related to specific conditions such as surficial layers with high concentrations in organic acids (Colin et al., 1993), or related to specific Zr-bearing phases, such as metamict zircons or volcanic glasses.

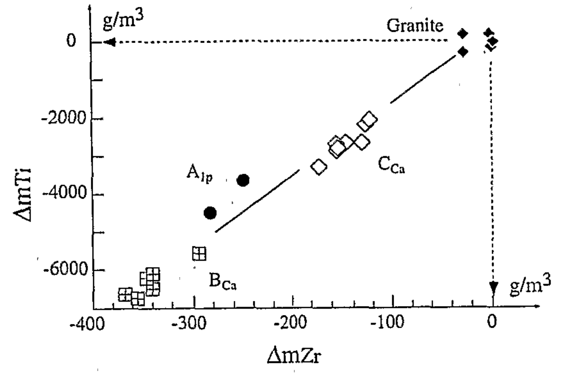

Fig. 8. Plot of the mass transfer of Ti vs. Zr, from isovolumeric mass-balance calculation. The linear correlation indicates that Ti and Zr, two classical immobile elements, are both depleted at the same rate. However, in the whole rock, Zr is located in zircon while Ti is associated with rutile or anatase.

4.2. Calcitization

By contrast with all other elements, Ca and Sr are imported massively from allochtonous sources during the calcitization process. The total inventory of calcium, between 3.7 and 0.3 m depth in the calcrete profile, corresponds to 415 kg/m^2. By comparison, the initial stock of Ca in a comparable volume of parent granite is only 155 kg/m^2, considering a calcium content in the fresh rock of 45.6 kg/m^3. Relics of the granite are present throughout the profile, suggesting that part of the authigenic Ca remains included in primary mineral phases. The measurements performed at different levels in the saprolitic discontinuous calcrete (C_{Ca}) show that 27 to 42% of Ca (i.e., 42 to 65 kg/m^2) had already

Fig. 7. Plot of Ti vs. calcium carbonate concentrations. Comparison of Ti values with those of Th and Zr. All concentrations are expressed in grams of element per unit volume of bulk sample.

been exported prior to the massive calcitization developed in the continuous calcrete layer. The quantity of Ca remaining in the residual silicates of the calcrete layers can be estimated from the difference between the bulk Ca content (given by ICP bulk measurements), and Ca in the calcitic matrix (given by calcimetry). This shows that only 15% to 29% of the original calcium remains in residual silicates within the saprolite (i.e., 23 to 45 kg/m^2). Weathering of this residue probably continues in the upper calcrete layers, but the resulting additional loss of calcium is completely masked by the massive precipitation of exogenic calcium carbonate. Assuming congruent dissolution, as suggested above from the discussion of the insoluble elements (Ti, Zr and Th), we estimate that only 8% to 42% (i.e., 12 to 65 kg/m^2) of the original Ca remains in the residual silicates of the upper calcrete layers (Fig. 9).

Some of the Ca released by the dissolution of the parent rock is clearly re-precipitated within the calcium carbonate. However, this fraction cannot be distinguished from the allochtonous input in the total Ca budget of the calcrete. By contrast, the percentage of authigenic Sr can be estimated from Sr isotope measurements, by taking advantage of the large difference of ^{87}Sr/^{86}Sr between the calcrete and the parent granite (Capo and Chadwick, 1993a,b; Fleischhauer and Dworkin, 1993; Quade et al., 1995). We have shown (Chiquet et al., 1999) that Sr in the Toledo calcrete has a ^{87}Sr/^{86}Sr ratio close to that of the local atmospheric fallout, thus, setting an upper limit of 5% on the proportion of Sr derived from the parent rock within the calcrete. From this result, and assuming that Sr and Ca have a similar geochemical behaviour, we estimate that 373 kg/m^2 of the calcium is of allochtonous origin in the calcite, while 17 kg/m^2 is autochtonous (Fig. 9). Therefore, only 15% of the Ca released by weathering of the original silicate minerals have been incorporated into the calcite.

Considering that 373 kg/m^2 of Ca (this study) and 315 mg/m^2 of Sr (Chiquet et al., 1999) are allochtonous, a [Ca]/[Sr] ratio of 1200 is calculated for the external input, similar to that of most calcareous lithologies. The Sr isotopic data reported in Chiquet et al. (1999) also suggest that the allochtonous Sr is mostly derived from aeolian transport of distant limestones. Indeed, no significant

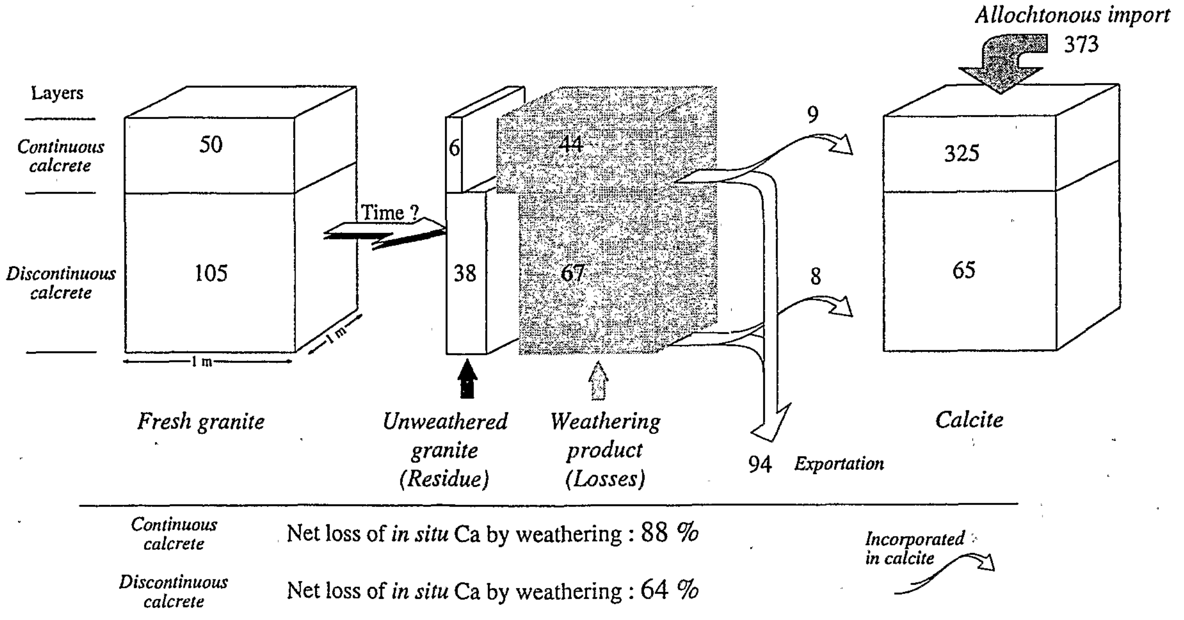

Fig. 9. Calcium inventories (kg/m^2) in the Gálvez calcrete profile. A clear distinction must be made between the continuous calcrete (0.3–1.4 m depth) and the discontinuous calcrete (1.4–3.7 m depth) layers.

carbonate formations with appropriate Sr isotopic composition are observed on the Toledo platform (Chiquet et al., 1999).

The downward transport and precipitation of this atmospheric deposit of calcium is ensured by percolating rainwaters, through the seasonal cycle described above. In the Toledo calcrete, field observations also reveal the presence of sub-horizontal calcitic laminations at the top of the continuous calcrete layer, reflecting lateral sub-surface circulation of the soil solutions. This generates a downslope evolution of the mineral sequence: calcium carbonate occurs successively along the slope, first as diffuse patches, then as loose nodular accumulations, and downhill as massive planar precipitates, while the proportion of parent mineral relics decreases.

In the studied profile, calcite has a unimodal vertical distribution at between 0.3 and 1.4 m depth. McDonald et al. (1996) suggested that this type of distribution results from a constant annual downward flux of soil-water, related to stable climatic conditions controlling the depth of calcite precipitation. By contrast, bimodal downward profiles of Ca carbonate content can be found in other sequences, where contrasted hydrodynamic regimes have taken place successively during the Holocene (McDonald et al., 1996).

The sensitivity of calcrete genesis to climate is also demonstrated by the absence of calcium carbonate precipitation in other palaeo-weathering profiles, which have developed on the same hercynian basement of the Toledo Mountains during the Neogene. These profiles, described by Molina et al. (1990, 1991), Vicente et al. (1991, 1997) and Martínez Lope et al. (1995) have been fossilized by Mio-Pleistocene sedimentary series (rañas), in the northern piedmont of the Toledo Mountains (Fig. 1). More humid climatic conditions must have prevailed during weathering of these rocks, in order to explain that calcrete precipitation did not occur in these sequences, in spite of similar parent rocks and topographic situation as those of the more recent facies studied in the present work.

5. Conclusions

The chemical budget of calcrete genesis is investigated on a typical profile developed on granite in the Toledo mountains, Central Spain. Field and petrographic observations demonstrate that calcitization and weathering of the granite are synchronous and interrelated processes, with a strict preservation of the initial structure and volume of the parent rock, both at the mineral scale and at a macroscopic scale throughout the profile. Iso-volume mass-balance calculation has been applied on major and trace element concentrations measured in this profile. With respect to the unweathered granite, the loss of material increases from the saprolite to the calcrete horizons, due to increasing weathering of the granite. Simultaneously, calcite precipitates due to highly alcaline conditions. A massive input of allochtonous calcium is required to account for the large increase of the calcium inventory. Significant Ti, Zr and Th chemical depletions are observed in the most Ca-rich part of the profile, which precludes using these elements as immobile for the mass budget calculations.

We estimate that 8–42% of the calcium initially present in the fresh granite remains stored in the residual silicates of the calcrete layers. This result, when coupled with previous Sr isotopic data, suggests that only 15% of the calcium released by weathering of the original silicate minerals have been incorporated into the calcite. Finally, a Ca/Sr mass ratio of 1200 is calculated for the allochtonous input. This suggests that the genesis of calcretes is related to the atmospheric fallout of calcareous dust, since a direct contribution from limestone formations seems very unlikely in this region.

Acknowledgements

This work was supported by the INSU-CNRS program Dynamique et Bilans de la Terre. Pr. B. Gilkes and Dr. E. Hamidi are acknowledged for helpful discussions.

References

Aristarain, L.F., 1971. On the definition of caliche genesis. Z. Geomorph. (NF) 15, 274–289.

Bech, J., Nahon, D., Paquet, H., Ruellan, A., Millot, G., 1980. Sur l'extension géographique et climatique des phénomènes d'épigénie par la calcite dans les encroûtements calcaires.

Exemple de la Catalogne. Compte Rendu de l'Académie des Sciences, Paris 291, 371–376.

Blum, J.D., Erel, Y., 1995. A silicate weathering mechanism linking increases in marine ^{87}Sr/^{86}Sr with global glaciation. Nature 373, 415–418.

Blum, J.D., Erel, Y., 1997. Rb–Sr isotope systematics of a granitic soil chronosequence: The importance of biotite weathering. Geochim. Cosmochim. Acta 61 (15), 3193–3204.

Blum, J.D., Erel, Y., Brown, K., 1994. ^{87}Sr/^{86}Sr ratios of Sierra Nevada stream waters: implications for relative mineral weathering rates. Geochim. Cosmochim. Acta 58, 5019–5025.

Boulet, R., 1974. Toposéquences de sols tropicaux en Haute-Volta: équilibres dynamiques et bioclimats. Thèse Sciences naturelles, Université de Strasbourg.

Brimhall, G.H., Chadwick, O.A., Lewis, C.J., Compson, W., Williams, I.S., Danty, K.J., Dietrich, W.E., Power, M.E., Hendricks, D., Bratt, J., 1992. Deformational mass transport and invasive processes in soil evolution. Science 255, 695–702.

Brimhall, G.H., Lewis, C.J., Ford, C., Bratt, J., Taylor, G., Warin, O., 1991. Quantitative geochemical approach to pedogenesis: importance of parent material reduction, volumetric expansion, and eolian influx in laterization. Geoderma 51, 51–91.

Capo, R.C., Chadwick, O.A., 1993a. Application of strontium isotopes to the mass balance of calcium in desert soils: eolian inputs versus in situ weathering. Fall Meet. AGU, San Fransisco, USA 74 (43), 263.

Capo, R.C., Chadwick,O.A., 1993b. Partitionning of atmospheric and silicates weathering sources in the formation of desert soil carbonate using strontium isotopes. Abstract with programs.

Chapman, R.W., 1974. Calcareous duri-crust in Al-Hasa, Saudi Arabia. Bull. Geol. Soc. Am. 85, 119–130.

Chiquet, A., Michard, A., Nahon, D., Hamelin, B., 1999. Atmospheric input vs. in situ weathering in the genesis of calcretes: a Sr study at Gálvez (Montes de Toledo, Spain). Geochim. Cosmochim. Acta, In press.

Colin, F., Brimhall, G.H., Nahon, D., Lewis, C.J., Baronnet, A., Danti, K., 1992. Equatorial rain forest lateritic mantles: a geomembrane filter. Geology 20, 523–526.

Colin, F., Vieillard, P., Ambrosi, J.P., 1993. Quantitative approach to physical and chemical gold mobility in equatorial rainforest lateritic environment. Earth Planet. Sci. Lett. 114, 269–285.

Dekayir, A., 1994. Etude de l'altération supergène d'un basalte alcalin quaternaire du Moyen Atlas (Maroc). Thèse de doctorat, Aix-Marseille III, 181 pp.

Drever, J.I., Hurcomb, D.R., 1986. Neutralization of atmospheric acidity by chemical weathering in an alpine drainage basin in the North Cascade Mountains. Geology 14, 221–224.

Ducloux, J., Laouina, A., Chaker, M., Dinel, H., 1990. Carbonate accumulation and weathering of the granitic substratum of Tanecherfi Basin, Northeastern Morocco. Catena 17, 493–508.

Durand, R., 1979. La pédogenèse en pays calcaire dans le Nord-Est de la France. Mem. Sci. Geol. 55, 1–198.

Fleischhauer, H.L., Dworkin, S.I., 1993. Geomorphic and pedogenic implications of the stable carbon, oxygen, and strontium isotopic composition of caliche, central Texas (abstract). Proceeding 394.

Gardner, L.R., 1980. Mobilization of Al and Ti during weathering — isovolumetric geochemical evidence. Chem. Geol. 30, 151–165.

Gardner, L.R., Kheruenromne, I., Chen, H.S., 1978. Isovolumetric geochemical investigation of a buried granite saprolite near Columbia S.C., U.S.A. Geochim. Cosmochim. Acta 42, 417–424.

Lasaga, A.C., 1984. Chemical kinetics of water–rock interactions. J. Geophys. Res. 89, 4009–4025.

Marion, G.M., Schlessinger, W.H., Fonteyn, P.J., 1985. Caldep: a regional model for soil CaCO$_3$ (caliche) deposition in South western deserts. Soil Sci. 139, 468–481.

Martínez Lope, M.J., Garcia Gonzales, M.T., Molina, E., 1995. Relationships between geomorphology and palaeoweatherings on the hercynian basement in Central Spain. A mineralogical and geochemical approach. Rev. Soc. Geol. España 8 (1-2), 126–136.

Mayer, L., McFadden, L.D., Harden, J.W., 1988. Distribution of calcium carbonate in desert soils: a model. Geology 16, 303–306.

McDonald, E.V., Pierson, F.B., Flerchinger, G.N., McFadden, L.D., 1996. Application of a soil–water balance model to evaluate the influence of Holocene climate change on calcic soils, Mojave desert, California, U.S.A. Geoderma 74, 167–192.

McFadden, L.D., Tinsley, J.C., 1985. Rate and depth of pedogenic-carbonate accumulation in soils: formulation and testing of a compartment model. Geol. Soc. Am., Spec. Pap. 203, 23–41.

Melfi, A.J., Subies, F., Nahon, D., Formoso, M.L.L., 1996. Zirconium mobility in bauxites of southern Brazil. J. South Am. Earth Sci. 9 (3/4), 161–170.

Merino, E., Nahon, D., Wang, Y., 1993. Kinetics and mass transfer of pseudomorphic replacement: application to replacement of parent material by Al, Fe, and Mn oxides during weathering. Am. J. Sci. 293, 135–155.

Millot, G., Bonifas, M., 1955. Transformations isovolumétriques dans les phénomènes de latérisation et bauxitisation. Bull. Serv. Carte Geol. Alsace Lorraine 8, 3–20.

Millot, G., Nahon, D., Paquet, H., Ruellan. A., Tardy, Y., 1977. L'épigénie des roches silicatées dans les encroûtements carbonatés en pays sub-aride, Anti-Atlas, Maroc. Sci. Geol. Bull. 30 (3), 129–152.

Milnes, A.R., 1992. Calcrete. In: Martini, I.P., Chesworth, W. (Eds.), Weathering Soils and Paleosoils. Elsevier, pp. 309–347.

Molina, E., Cantano, M., Vicente, M.A., Garcia Rodriguez, P., 1990. Some aspects of paleoweathering in the iberian hercynian massif. Catena 17, 333–346.

Molina, E., Garcia Gonzales, M.T., Espejo, R., 1991. Study of paleoweathering on the spanish hercynian basement Montes de Toledo (Central Spain). Catena 18, 345–354.

Monger, H.C., Daugherty, L.A., 1991a. Pressure solution: possible mechanism for silicate grain dissolution in a petrocalcic horizon. Soil Sci. Am. J. 55, 1625–1629.

Monger, H.C., Daugherty, L.A., 1991b. Neoformation of palygorskite in a Southern New Mexico aridosol. Soil Sci. Am. J. 55, 1646–1650.

Murphy, S.F., Brantley, S.L., Blum, A.E., White, A.F., Dong, H., 1998. Chemical weathering in a tropical watershed, Luquillo Mountains, Puerto Rico: II. Rate and mechanism of biotite weathering. Geochim. Cosmochim. Acta 62 (2), 227–243.

Nagtegaal, P.J.C., 1969. Microtextures in recent and mineral paragenesis in sediments. Leid. Geol. Meded. 42, 131–142.

Nahon, D., Paquet, H., Ruellan, A., Millot, G., 1975. Encroûtements calcaires dans les altérations des marnes éocènes de la falaise de Thiès (Sénégal); Organisation morphologique et minéralogie. Bull. Sci. Geol. 28 (1), 29–46.

Nahon, D., 1976. Cuirasses ferrugineuses et encroûtements calcaires au sénégal et en Mauritanie. Systèmes évolutifs, structures, relais et coexistence. Mem. Sci. Geol. 44, 232 pp.

Nahon, D., 1991. Introduction to the Petrology of Soils and Chemical Weathering. 313 pp.

Nahon, D., Merino, E., 1996. Pseudomorphic replacement versus dilation in laterites: petrographic evidence, mechanisms, and consequences for modelling. J. Geochem. Explor. 57, 217–225.

Nahon, D., Merino, E., 1997. Pseudomorphic replacement in tropical weathering: evidence, geochemical consequences, and kinetic–rheological origin. Am. J. Sci. 297, 393–417.

Nesbitt, H.W., 1979. Mobility and fractionation of rare earth elements during weathering of a granodiorite. Nature 279, 206–210.

Nesbitt, H.W., Markovics, G., Price, R.C., 1980. Chemical processes affecting alkalis and alkaline earths during continental weathering. Geochim. Cosmochim. Acta 44, 1659–1666.

Nesbitt, H.W., Wilson, R.E., 1992. Recent chemical weathering of basalts. Am. J. Sci. 292, 740–777.

Paquet, H., 1983. Stability, instability and significance of attapulgite in the calcretes of mediterranean and tropical areas with marked dry season. Mem. Sci. Geol. 72, 131–140.

Paquet, H., Ruellan, A., 1993. Epigénie et encroûtements calcaires (calcrètes). Coll. ''Sédimentologie et Géochimie de la Surface'' à la mémoire de Georges MILLOT. pp. 1–18.

Quade, J., Chivas, A.R., McCulloch, M.T., 1995. Strontium and carbon isotope tracers and the origins of soil carbonate in South Australia and Victoria. Palaeogeogr. Palaeoclimatol. Palaeoecol. 113, 104–117.

Reheis, M.C., 1988. Pedogenic replacement of aluminosilicate grains by $CaCO_3$ in Ustollic Haplargids, South-Central Montana, USA. Geoderma 41, 243–261.

Ruellan, A., 1971. Les sols à profils calcaires différenciés des plaines de la basse Moulouya, Maroc Oriental. Mem. ORSTOM 54, 302 pp.

Trescases, J.J., 1975. L'évolution géochimique supergène des roches ultrabasiques en zone tropicale. Formation des gisements nickelifères de Nouvelle-Calédonie. Mem. ORSTOM 78, 259 pp.

Vaudour, J., 1979. La région de Madrid: altérations, sols et paléosols. Thèse d'état, Aix-en-Provence, 390 pp.

Velbel, M.A., 1985. Geochemical mass-balances and weathering rates in forested watersheds of the southern Blue Ridge. Am. J. Sci. 285, 904–930.

Vicente, M.A., Elsass, F., Molina, E., Robert, M., 1997. Palaeoweathering in slates from the Iberian Hercynian Massif (Spain): investigation by TEM of clay mineral signatures. Clay Miner. 32, 435–451.

Vicente, M.A., Molina, E., Espejo, R., 1991. Clays in paleoweathering processes: study of a typical weathering profile in the hercynian basement in the Montes de Toledo (Spain). Clay Miner. 26, 81–90.

Wang, Y., Nahon, D., Merino, E., 1994. Dynamic model of the genesis of calcretes replacing silicate rocks in semi-arid regions. Geochim. Cosmochim. Acta 58 (23), 5131–5145.

White, A.F., Blum, A.E., Shulz, M.S., Bullen, T.D., Harden, J.W., Peterson, M.L., 1996. Chemical weathering rates of a soil chronosequence on granitic alluvium: I. Quantification of mineralogical and surface area changes and calculation of primary silicate reactions rates. Geochim. Cosmochim. Acta 60 (14), 2533–2550.

Wright, V.P., Platt, N.H., Mariott, S.B., Beck, V.H., 1995. A classification of rhizogenic (root-formed) calcretes, with examples from the Upper Jurassic–Lower Cretaceous of Spain and Upper Cretaceous of southern France. Sediment. Geol. 100, 143–158.